

NUMERICAL EVALUATION OF UPSTREAM BEND INSTALLATION EFFECTS ON FULLY DEVELOPED FLOW PROFILES AIMING ULTRASONIC FLOW METERING

Ramon Silva Martins, ramonsmartins@gmail.com

Rogério Ramos, ramosrogerio@hotmail.com

LFTC, PPGEM, Department of Mechanical Engineering, Universidade Federal do Espírito Santo.

Av. Fernando Ferrari, 514. Vitória - ES CEP 29075-910

Telephone number: +55 27 40092641 / Fax: +55 27 40092650

Abstract. Oil and gas flows need accurate rates measurement since they are stated by law. In such industries fields some pipe effects are usual to be faced, due to installation connectors for example. Hence flow disturbances occur and measurement accuracy may be committed. On the other hand, ultrasonic flow measurement technology depends on being installed at a tube section where fully developed flow is established. The paper presents, specifically, a preliminary evaluation of upstream bend effects on flow profiles at metering section. A numerical approach has been used in order to estimate the entrance length and fully developed flow definition via computational fluid dynamics (CFD). Standard $k - \epsilon$ turbulence model has been used to all simulations. Reynolds number is defined as 1×10^5 and previous results are graphically shown and commented.

Keywords: installation effects, bend, flow metering, numerical simulation, ultrasonic flow meter

1. INTRODUCTION

Flow meters calibration represents an important issue to oil and gas industry, where accurate flow measurements are required and national regulations describes the proceedings for operational and custody metering. These documents, such as AGA (2007) and ANP/INMETRO (2000), points out ultrasonic flow meters (UFM's) as a suitable technology for oil and gas metering. Still, the conditions for accurate flow measurements may be not reliable due to several installation obstacles, such as bends, valves and diameter step changes. In many cases, due to available space, such obstacles are close to the metering section causing flow disturbances. Since the majority of flow meters depends on fully developed flow condition at these locations, the flow metering is thus compromised in such situations.

Scientific and technological community has been evaluating flow disturbances patterns and consequences as well as methods to diminish flow measurement errors and uncertainties. Ruppel and Peters (2004) and Mickan *et al.* (1997) identify downstream flow patterns of typical pipe installation by means of experiments. Hilgenstock and Ernst (1996) compare computational fluid dynamics (CFD) results and experiments, pointing numerical simulations as an interesting tool for meters calibration and diagnostic. Holm *et al.* (1995) proposed the calculation of a numerical k factor in order to evaluate various installation effects on UFM's.

On the other side, according to its measurement principle, UFM is relatively sensitive to flow profile disturbances and this dependence can be better understood by knowing its basic configuration and operational fundamentals.

A UFM is composed, at least, by two ultrasonic transducers transmitting and receiving ultrasonic pulses through the fluid, so composing a single acoustic channel with a certain inclination (α) relative to the pipe axis (Fig. 1).

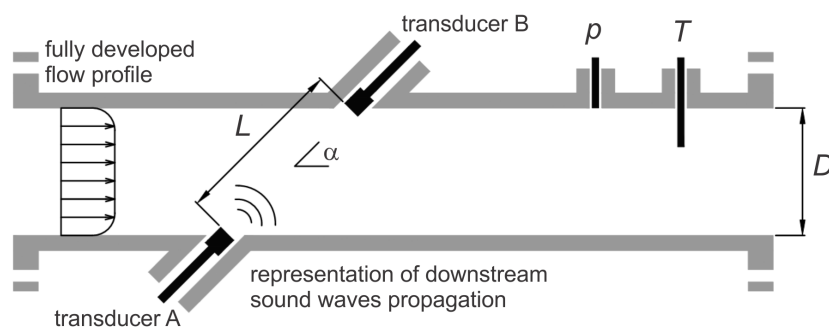


Figure 1. Ultrasonic flow meter basic scheme.

Supposing a non-flow situation, the transit time - time which the ultrasonic pulse takes to travel from a transducer to the other - and the distance between the transducers (L) may give the sound propagation velocity in the fluid (c). Once there is a flow velocity field, transit times become different due to the consequent signal deviation. That makes downstream pulse transit time, which goes from transducer A to B (t_{AB}), shorter than upstream pulse, which goes from transducer B

to A (t_{BA}), since the pulse propagates against the flow. Calculation of transit mean velocities (u_{AB} and u_{BA}) are possible and they are given by Eqs. (1) and (2), considering that transducers distance (L), diameter (D) and transit times (t_{AB} and t_{BA}), are known variables.

$$u_{AB} = \frac{L}{t_{AB}} = c + \bar{u}_{SP} \cos \alpha \quad (1)$$

$$u_{BA} = \frac{L}{t_{BA}} = c - \bar{u}_{SP} \cos \alpha \quad (2)$$

\bar{u}_{SP} is the flow mean velocity over the sound path. The unknowns \bar{u}_{SP} and c can be found by solving the algebraic system of Eqs. (1) and (2) and the result is shown in Eqs. (3) and (4).

$$c = \frac{D}{2 \sin \alpha} \left(\frac{t_{AB} + t_{BA}}{t_{AB} t_{BA}} \right) \quad (3)$$

$$\bar{u}_{SP} = \frac{D}{\sin 2\alpha} \left(\frac{t_{AB} - t_{BA}}{t_{AB} t_{BA}} \right) \quad (4)$$

Due to their measurement principle, ultrasonic flow meters calculate c and \bar{u}_{SP} , nevertheless the flow cross sectional mean velocity (\bar{u}_m) is useful on flow rate calculation. \bar{u}_m depends on flow profile geometry and a correction factor (k) which consider fully developed flow, is used to obtain it from \bar{u}_{SP} as shown in Eq. (5) (Carlander and Delsing, 2000; Mylvaganam, 1989).

$$\bar{u}_m = k \bar{u}_{SP} \quad (5)$$

The aim of the paper is to compare the behavior of velocity profile obtained by a straight tube against the disturbed profile generated by an upstream bend, exposed to the same flow parameters. Two distinct curvature radii have been explored. The classical Nikuradse (1966) profile (as indicated by AGA (2007) and ABNT (2010)) is compared against modern approaches, as well.

2. MATHEMATICAL MODEL AND NUMERICAL SIMULATION PARAMETERS

This section presents the governing equations used to mathematical modelling, the boundary conditions, geometry configurations, meshes and the numerical method used to obtain all follow results.

2.1 Conservation equations

Considering stationary flow, fluid incompressibility and constant viscosity conditions, the turbulent flow may be predicted by the mass and the momentum conservation equations. These equations are presented in indicial notation by Eqs. (6) and (7), respectively.

$$\frac{\partial \rho u_i}{\partial x_i} = 0 \quad (6)$$

$$\rho \frac{\partial (\bar{u}_i \bar{u}_j)}{\partial x_i} = - \frac{\partial p}{\partial x_j} + \frac{\partial}{\partial x_i} \left[(\mu + \mu_T) \left(\frac{\partial \bar{u}_i}{\partial x_j} + \frac{\partial \bar{u}_j}{\partial x_i} \right) \right] \quad (7)$$

Where ρ is the fluid density, u_i is the velocity component in direction i , \bar{u}_i is the turbulent mean velocity in direction i , μ is the dynamic viscosity and μ_T is the turbulent viscosity, given by the turbulence model.

2.2 Turbulence modeling

The momentum equation considering turbulence needs additional equations to be solved. These equations come from the turbulence model. In this paper the standard $k - \varepsilon$ model has been used, as well as the Boussinesq hypothesis, which considerate the turbulent viscosity (μ_T) for the relation between the Reynolds stresses tensor and the turbulent mean velocity, as shown in Eq. (8).

$$\tau_{Tij} = \mu_T \left(\frac{\partial \bar{u}_i}{\partial x_j} + \frac{\partial \bar{u}_j}{\partial x_i} \right) \quad (8)$$

Where τ_{Tij} is the Reynolds stresses tensor. Two extra transport equations must be solved in order to obtain μ_T . Transport equations for k (turbulence kinetic energy) and for ε (turbulence eddy dissipation) are Eqs. (9) and (10), respectively.

$$\rho \frac{\partial (\bar{u}_i k)}{\partial x_j} = \frac{\partial}{\partial x_j} \left[\left(\mu + \frac{\mu_T}{\sigma_k} \right) \frac{\partial k}{\partial x_i} \right] + P_k + \rho \varepsilon \quad (9)$$

$$\rho \frac{\partial(\bar{u}_i \varepsilon)}{\partial x_j} = \frac{\partial}{\partial x_j} \left[\left(\mu + \frac{\mu_T}{\sigma_\varepsilon} \right) \frac{\partial k}{\partial x_i} \right] + \frac{\varepsilon}{k} (C_{\varepsilon 1} P_k + C_{\varepsilon 2} \rho \varepsilon) \quad (10)$$

Where P_k is obtained from Eq. 11 and σ_k , σ_ε , $C_{\varepsilon 1}$ and $C_{\varepsilon 2}$ are constants of the model and their values are presented in Tab. 1.

$$P_k = \mu_T \frac{\partial \bar{u}_i}{\partial x_j} \left(\frac{\partial \bar{u}_i}{\partial x_j} + \frac{\partial \bar{u}_j}{\partial x_i} \right) \quad (11)$$

The turbulent viscosity (μ_T) is finally obtained from Eq. 12.

$$\mu_T = C_\mu \rho \frac{k^2}{\varepsilon} \quad (12)$$

Where C_μ is a constant of the model and its value is also presented in Tab. 1. (Versteeg and Malalasekera, 2007)

Table 1. Constants of the standard $k - \varepsilon$ model.

σ_k	σ_ε	$C_{\varepsilon 1}$	$C_{\varepsilon 2}$	C_μ
1.0	1.3	1.44	1.92	0.09

2.3 Geometries and meshes

At first, a straight pipe flow has been simulated in order to check fully development flow reproducibility. This basic geometry is illustrated in Fig. 2. Once straight pipe case has been checked, single bend cases have been configured as shown in Fig. 3. In all cases internal diameter of 300 mm has been used. Curvature radii of 0.0D and 1.0D have been set as well as the same 100D (30,000 mm) downstream straight pipe length.

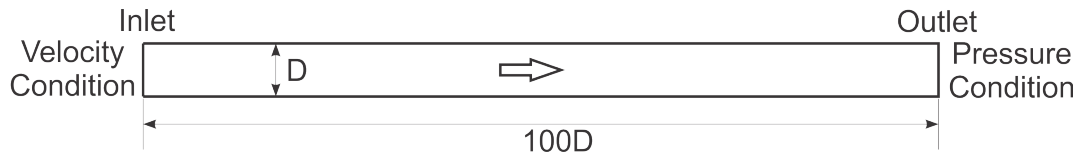


Figure 2. Straight pipe configuration.

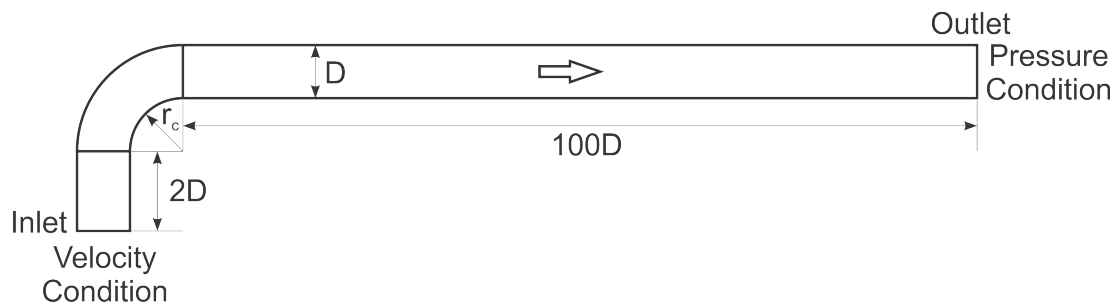


Figure 3. Single bend pipe configuration.

Hexahedron dominant meshes have been used for numerical solutions. Previously tetrahedron dominant meshes (unstructured) have been tested. Such unstructured meshes still influenced the results even at computer's memory limit. Hexahedral meshes tend to be composed by more nodes than elements. Since the mesh refinement criteria used was based in nodal points, the hexahedral mesh has provided greater node numbers. Hence mesh convergence could be observed.

Figure 4 exemplifies the meshes tested in this paper. As can be seen, meshes 3 to 6 use wall refinement with prismatic volumes aiming better representation of wall effects.

2.4 Boundary conditions and fluid model

Boundary conditions are also necessary to solve the of governing equations system. Here, smooth wall and no slip condition have been considered for pipe wall. Inlet condition has been set as normal uniform velocity profile so that desired Reynolds numbers were achieved. Medium turbulence intensity at entrance domain has been supposed. Average static pressure (in the same value of reference pressure, i.e., 1 atm) has been set as overall outlet condition. Air at 25°C has been considered in all cases. Table 2 resumes all input parameters.

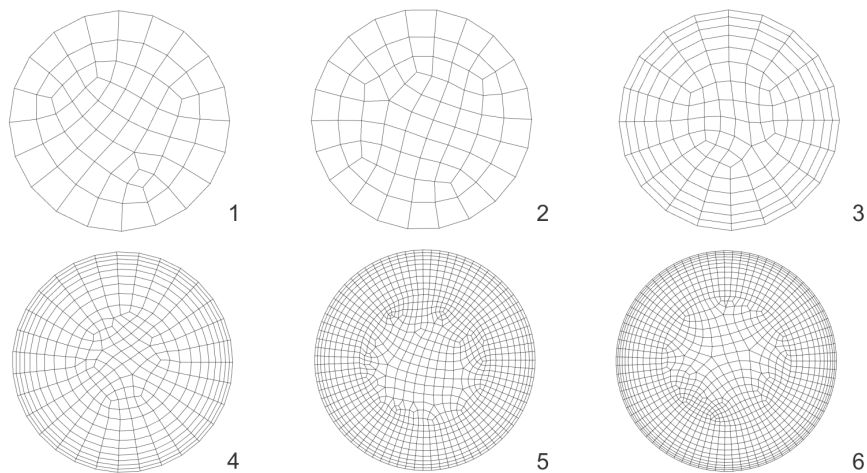


Figure 4. Hexahedral meshes used for numerical solution.

Table 2. Synthesis of boundary conditions and fluid parameters.

Fluid	Air at 25°C
Density	1.185 kg/m ³
Dynamic Viscosity	1.831x10 ⁻⁵ kg/m.s
Reference Pressure	1 atm
Turbulence Intensity at Entrance	Medium
Average Static Pressure at Outlet	1 atm
Wall Roughness	Smooth Wall
Wall Condition	No Slip
Reynolds Number	1x10 ⁵

2.5 Numerical solution

Commercially available CFD code has been used to achieve numerical solution (Ansys, Inc., 2010b). The software uses the Finite Volume Method conjugated with Multigrid accelerated Incomplete Lower Upper factorization technique for solving the discrete governing equations algebraic system. As convergence criteria, the root mean square (RMS) residuals of the linear solution of discrete governing equations are controlled to be smaller than 1x10⁻⁴. The advection scheme chosen was the High Resolution (Ansys, Inc., 2010a). All runs were performed by a PC equipped with Quad Core processor 2.4 GHz, 4.0 Gb memory and 8 Mb cache.

3. RESULTS AND DISCUSSION

Main results of all simulations are now presented and discussed. First of all, Tab. 3 presents some features as well as the respective CPU time for tested meshes, as cited in section 2.3. As can be seen, the latter mesh running is represented by mesh # 6, consisting by more than 3 million nodes and expending 6 hours of CPU time using 4 processors, approximately.

Table 3. Meshes features and CPU time.

Mesh#	Nodes	CPU time [h:min:s]	Number of processors	Wall refinement
1	48,4888	0:04:01.766	1	No
2	103,286	0:10:36.359	1	No
3	234,156	0:26:32.422	1	Yes
4	826,117	1:42:18.266	1	Yes
5	2,892,771	7:45:22.250	1	Yes
6	3,076,230	6:16:20.312	4	Yes

On the other hand, such computation effort points to a relatively good convergence of mesh # 6 to the velocity at pipe center, in comparison with other meshes, as can be checked in Fig. 5. The figure also indicates that velocity *u* at pipe

center reaches stability at 60D, approximately.

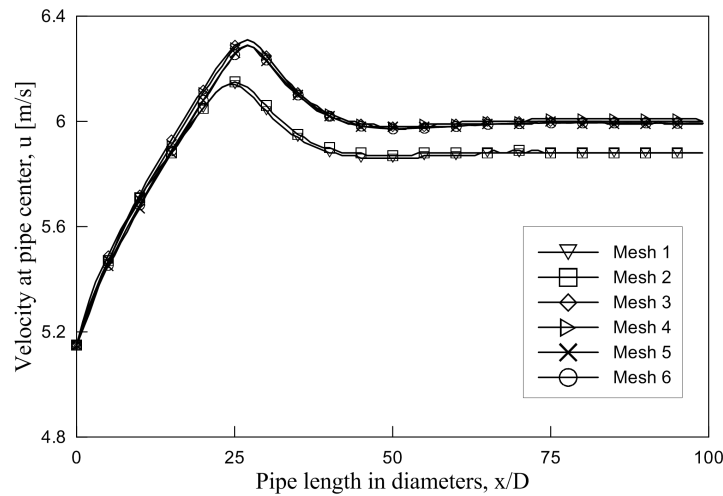


Figure 5. u velocity at pipe center for straight pipe case.

Comparison of fully developed flow profile at 80D for tested meshes is presented in Fig. 6 and, once again, mesh # 6 presents a good convergence when compared to the tested meshes.

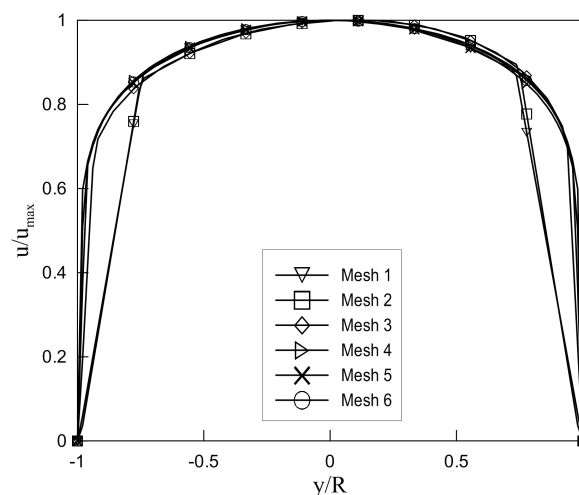


Figure 6. u velocity profile for all tested meshes at 80D for straight pipe case.

The validation of present fully developed profile can be seen in Fig. 7, when the present profile is compared to consolidated profiles which can be found in the open specialized literature. In the present case, the comparison is carried out against the profile proposed by De Chant (2005) and the classical profile of Nikuradse (1966).

Nikuradse (1966) profile is used here since it is cited by AGA (2007) and ABNT (2010) as the fully developed profile to be achieved by turbulent flows. On the other hand, De Chant (2005) work brings updated information about the behavior of flow profile in fully developed condition.

As can be observed, the present proposition reaches good agreement to De Chant (2005) profile, indicating that the procedure adopted here is valid and up to date, considering modern developments. On the other hand, the classical profile of Nikuradse (1966) points to slower velocities. Once it has been used as the reference turbulent fully developed profile by AGA (2007) and ABNT (2010), the results may indicate a need for further revision of such documents, at least.

In Fig. 8 it is demonstrated the development of flow profile at distinct straight tube lengths: 20D, 40D, 60D and 80D. Relative deviations of such profiles are tabulated at Tab. 4.

As can be noted from Tab. 4, maximum relative deviation of -2.55% occur between 20D and 40D at $y/R = -0.25$ and decreases until the minimum deviation estimated as -0.01% between 60D and 80D at $y/R = 0.75$. Such behavior can be better visualized in Fig. 9 where it is easy to notice that relative deviations at 20-40D profiles are higher when compared to 80-100D profiles, considering all positions.

It should be considered that, if the k -factor (Eq. 5) is related to flow profile and it is computed on UFM flow meters considering a fully developed flow so, such deviations impacts directly on the flow measurement.

Once the proposed profile at 80D is accept as a viable profile, its symmetry can be checked as shown in Fig. 10.

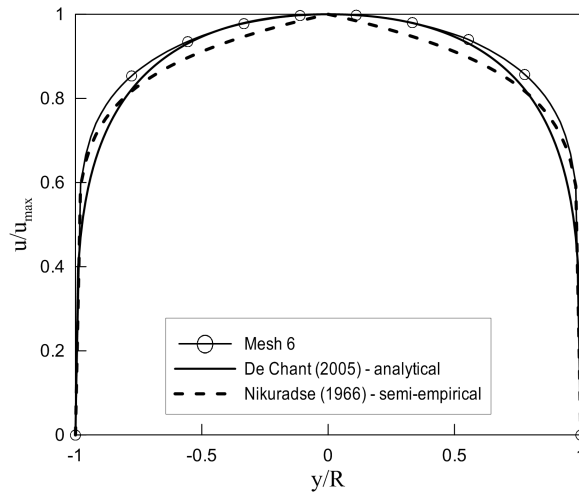


Figure 7. Comparison of u velocity profile for converged mesh at 80D for straight pipe case against De Chant (2005) and Nikuradse (1966).

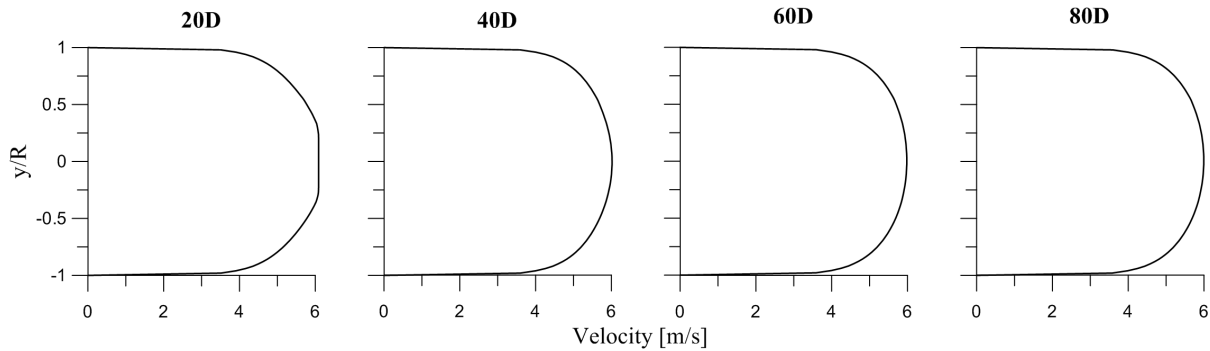


Figure 8. Converged u velocity profiles at several straight lengths.

Table 4. Deviations concerned to velocity profiles development.

y/R	u [m/s]		Relative Deviation									
	20D	40D		40D	60D		60D	80D		80D	100D	
-0.75	5.133	5.183	0.96%	5.183	5.188	0.10%	5.188	5.180	-0.14%	5.180	5.185	0.10%
-0.50	5.786	5.685	-1.59%	5.685	5.696	0.01%	5.696	5.693	-0.04%	5.693	5.702	0.16%
-0.25	6.085	5.934	-2.55%	5.934	5.910	-0.40%	5.910	5.916	0.10%	5.916	5.925	0.14%
0.00	6.088	6.018	-1.17%	6.018	5.982	-0.59%	5.982	5.994	0.20%	5.994	6.000	0.09%
0.25	6.080	5.933	-2.49%	5.933	5.917	-0.26%	5.917	5.928	0.18%	5.928	5.930	0.04%
0.50	5.784	5.695	-1.55%	5.695	5.708	0.22%	5.708	5.713	0.08%	5.713	5.711	-0.02%
0.75	5.132	5.186	1.04%	5.186	5.202	0.32%	5.202	5.202	-0.01%	5.202	5.196	-0.11%

Following the same methodology for straight tubes, now it is analysed the effect of an upstream bend presenting curvature radius (90° elbow) in order to reach a fully developed velocity profile.

Such methodology leads to Fig. 11 where, once again, it can be viewed the development of the velocity at pipe center, considering several distinct meshes. From Fig. 11, mesh # 10 is chosen as the one which provides the best convergence.

In the same way, in Fig. 12, mesh # 14 provides converged profiles in the case of upstream bend $r_c = 1.0D$, as shown in Fig. 3. It has to be observed that in such case, the profile reach stability just at 60D of straight pipe.

In order to better understand the effect of such installation features on the velocity behavior, the profiles obtained from straight tube, bends with 0.0D and 1.0D curvature radii are plotted together, as shown in Fig. 13.

In Fig. 13, it is noticed that all studied cases presented ($r_c = 0.0D$, $r_c = 1.0D$ and straight tube) collapses on the fully developed flow at 80D straight length. The agreements are not so good to shorter duct lengths. But, contrary of the statements contained in AGA (2007), ABNT (2010) as well as technical brochures from some UFM manufactures, the expected profiles are far from fully developed at such positions. This behavior indicates that in such situation, which means development lengths of less than 60D, it should be considered the installation of multipath ultrasonic flow meters instead of single path UFM, since the former are capable to deal with such asymmetries on flow profiles. Flow conditioners

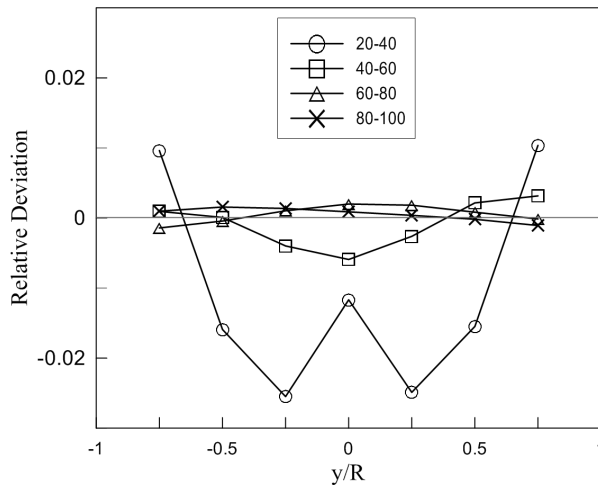


Figure 9. Relative deviation analysis.

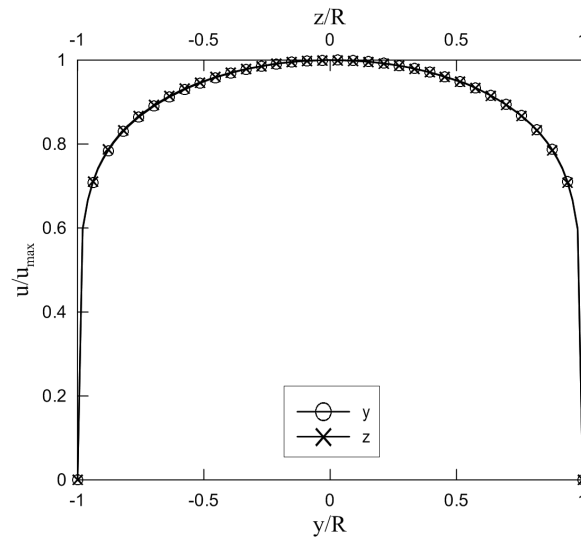


Figure 10. u velocity profile symmetry for converged mesh at 80D for straight pipe case.

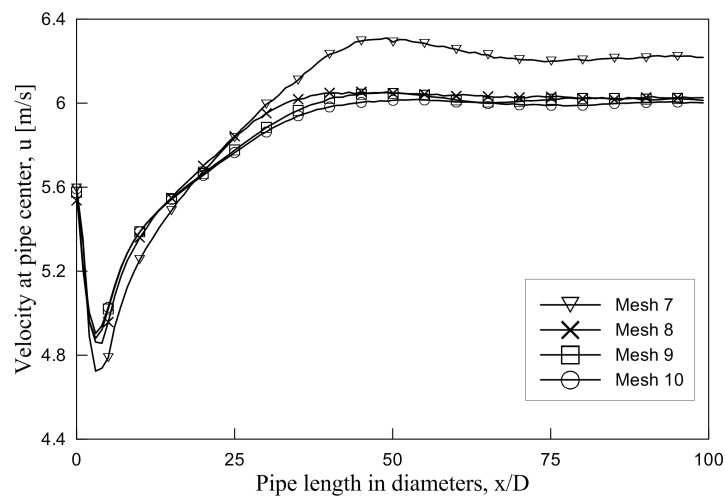


Figure 11. u velocity at pipe center for upstream single elbow - $r_c = 0.0D$.

installation could be considered.

An interesting aspect to be considered is the possibility to deal with such flow asymmetries by a new proposition of k -factor, presented in Eq. 5, which could be estimated by numerical way (Holm *et al.*, 1995) for a custom tubing configuration. This approach might permit quantifying any possible deviation on the analytical k -factor for both straight

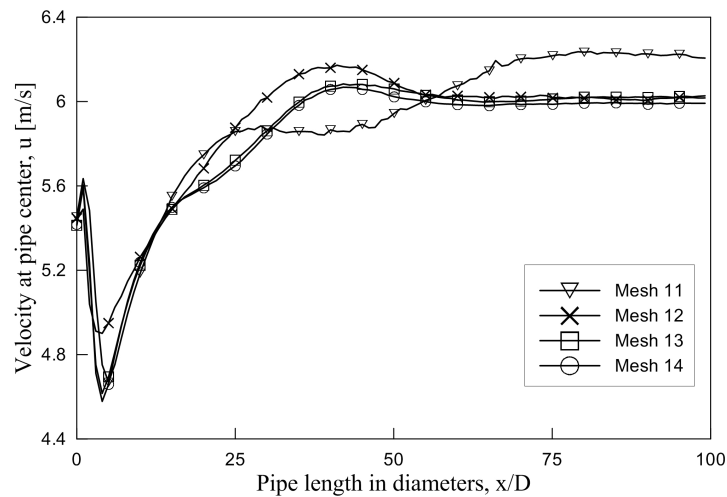


Figure 12. u velocity at pipe center for upstream single elbow - $r_c = 1.0D$.

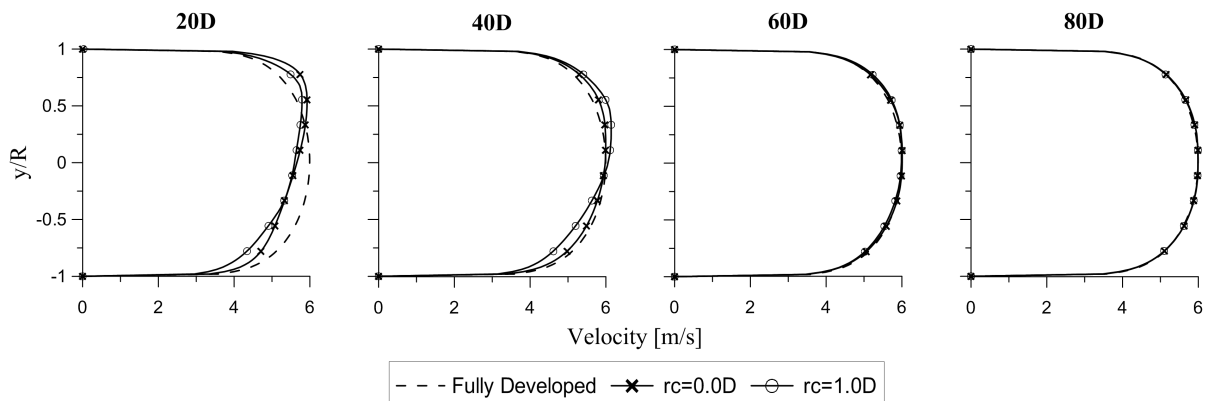


Figure 13. u velocity profiles for converged meshes at several straight lengths - $r_c = 0.0D$, $r_c = 1.0D$ and straight tube.

and curved pipe configurations when compared to the numerical k -factor. This proposition is already in progress and the numerical k -factor for several Reynolds numbers can be found in (Martins and Ramos, 2011). The application of such methodology in single and double bend configurations is a goal for future research work.

4. FINAL REMARKS

Numerical simulations using CFD techniques have presented a fully developed flow for straight tube and compared to distinct upstream bend configuration: $r_c = 0.0D$ and $r_c = 1.0D$. Classical velocity profiles for fully developed condition are criticized against modern numerical proposals.

Statements taken from AGA (2007) and ABNT (2010) about fully developed flow on UFM's are also criticized and a revision of such documents should be considered.

A new methodology for k -factor computation is commented as a goal for future research work, considering the previous developments stated by the present work.

5. ACKNOWLEDGEMENTS

The authors would like to express their acknowledgements to Programa de Recursos Humanos - PRH of Agência Nacional de Petróleo, Gás Natural e Biocombustíveis - ANP for financing this project and for the grant, as well as to Laboratório de Fenômenos de Transporte Computacional - LFTC/UFES for the use of its computational facilities.

6. REFERENCES

- ABNT, 2010. "ABNT NBR 15855:2010 - Medição de gás por medidores do tipo ultra-sônicos multitrajetórias". Norma brasileira, Associação Brasileira de Normas Técnicas, Rio de Janeiro, Brazil.
- AGA, 2007. "Measurement of gas by multipath ultrasonic meters". Report No. 9, American Gas Association, Washington, DC, USA.

- ANP/INMETRO, 2000. “Portaria Conjunta ANP/INMETRO N° 1”. 20.06.2011 - DOU - Diário Oficial da União.
- Ansys, Inc., 2010a. “ANSYS CFX-Solver Theory Guide”. Canonsburg, PA, USA.
- Ansys, Inc., 2010b. “ANSYS CFX™ Version 13.0”.
- Carlander, C. and Delsing, J., 2000. “Installation effects on an ultrasonic flow meter with implications for self diagnostics”. *Flow Measurement and Instrumentation*, Vol. 11, No. 2, pp. 109 – 122. ISSN 0955-5986. doi:10.1016/S0955-5986(00)00005-4.
- De Chant, L.J., 2005. “The venerable $1/7^{th}$ power law turbulent velocity profile: a classical nonlinear boundary value problem solution and its relationship to stochastic processes”. *Applied Mathematics and Computation*, Vol. 161, No. 2, pp. 463 – 474. ISSN 0096-3003. doi:10.1016/j.amc.2003.12.109.
- Hilgenstock, A. and Ernst, R., 1996. “Analysis of installation effects by means of computational fluid dynamics – CFD vs experiments?” *Flow Measurement and Instrumentation*, Vol. 7, No. 3-4, pp. 161 – 171. ISSN 0955-5986. doi: 10.1016/S0955-5986(97)88066-1. Optical Methods in Flow Measurement.
- Holm, M., Stang, J. and Delsing, J., 1995. “Simulation of flow meter calibration factors for various installation effects”. *Measurement*, Vol. 15, No. 4, pp. 235 – 244. ISSN 0263-2241. doi:10.1016/0263-2241(95)00007-8.
- Martins, R.S. and Ramos, R., 2011. “Uma abordagem numérica para o cálculo de fator de correção de medidores de vazão por ultrassom”. *Submitted to the 6º Congresso Brasileiro de Pesquisa e Desenvolvimento em Petróleo e Gás*.
- Mickan, B., Wendt, G., Kramer, R. and Dopheide, D., 1997. “Systematic investigation of flow profiles in pipes and their effects on gas meter behaviour”. *Measurement*, Vol. 22, No. 1-2, pp. 1 – 14. ISSN 0263-2241. doi:10.1016/S0263-2241(97)00053-5.
- Mylvaganam, K., 1989. “High-rangeability ultrasonic gas flowmeter for monitoring flare gas”. *IEEE Transactions on Ultrasonics Ferroelectric and Frequency Control*, Vol. 36, No. 2, pp. 144 – 149.
- Nikuradse, J., 1966. “Laws of turbulent flow in smooth pipes”. NASA TT F-10, 359, National Aeronautics and Space Administration, Washington, USA. Translated from ‘Gesetzmässigkeiten der turbulenten Strömung in glatten Rohren’ *Forsch. Arb. Ing.-Wes.* No. 356 (1932) .
- Ruppel, C. and Peters, F., 2004. “Effects of upstream installations on the reading of an ultrasonic flowmeter”. *Flow Measurement and Instrumentation*, Vol. 15, No. 3, pp. 167 – 177. ISSN 0955-5986. doi: 10.1016/j.flowmeasinst.2003.12.004. Ultrasonic Flowmetering.
- Versteeg, H.K. and Malalasekera, W., 2007. *An Introduction to Computational Fluid Dynamics - The Finite Volume Method*. Pearson Education Limited, Essex, England.

7. RESPONSIBILITY NOTICE

The authors are the only responsible for the printed material included in this paper.